Calculated Band Profiles of the OH-Stretching Transitions in Water Dimer

Anna L. Garden

Department of Chemistry, University of Otago, P.O. Box 56, Dunedin 9054, New Zealand

Lauri Halonen

Laboratory of Physical Chemistry, P.O Box 55, FIN-00014 University of Helsinki, Finland

Henrik G. Kjaergaard*

Department of Chemistry, University of Otago, P.O. Box 56, Dunedin 9054, New Zealand, and The Lundbeck Foundation Center for Theoretical Chemistry, Department of Chemistry, Aarhus University, DK-8000, Aarhus C, Denmark

Received: March 6, 2008; Revised Manuscript Received: April 22, 2008

We have calculated the band profiles of the OH-stretching fundamental and overtone transitions in the proton donor unit of the water dimer complex. We have used a local mode Hamiltonian that includes both OH-stretching and OO-stretching motion but separates these adiabatically. The variation of OH-stretching frequency and anharmonicity with OO displacement from equilibrium contributes to the effective OO-stretching potentials for each OH-stretching state. The resulting OO-stretching energy levels and wave functions are used to simulate the vibrational profile of each OH-stretching transition. The coupled cluster with singles, doubles, and perturbative triples ab initio method with an augmented triple-ζ correlation consistent basis set has been used to obtain the necessary parameters, potentials, and dipole moment functions. We find that the OO-stretching transitions associated with a given hydrogen bonded OH-stretching transition are spread significantly and this spread increases with overtone. The spread is minor for the free OH-stretching transition. The inclusion of the OO-stretching mode has a limited effect on the overall OH-stretching band intensity.

Introduction

Water vapor is a major absorber of visible and near-infrared radiation in Earth's atmosphere. However, there is considerable absorption that cannot be accounted for by the rovibrational transitions of the gaseous water monomer.[1,2] The hydrogen-bonded water dimer has been proposed to contribute to this excess absorption.[1–5] Despite a plethora of theoretical and experimental studies on the spectroscopy of the water dimer, there is still much debate as to the precise role that water dimers play in the global radiation budget.

Most of the experimental spectra of water dimer have been in the fundamental or low overtone OH-stretching spectral regions. The frequency of the fundamental and first overtone OH-stretching transitions in water dimer have been determined by matrix isolation, helium droplet, gas phase, and jet-cooled infrared studies.[1,2,6–16] These experiments have been supported by various theoretical calculations.[3,4,17–23] Experimental intensities are more scarce, with relative intensities available from matrix isolation experiments and a few absolute intensities from the recent He droplet experiment.[16]

In addition to the position and intensity, knowledge of the shape and width of the individual absorption bands is required to accurately simulate the absorption spectrum of water dimer for assessment of its atmospheric impact. Most of the vibrational spectroscopy of water dimer is limited to nonequilibrium jet-cooled and matrix isolation experiments and as such provide limited information on the shape and width of the absorption bands at ambient temperatures.

There have been three recently reported measurements of vibrational transitions in water dimer at ambient temperatures.[1,2,24] In the 5000−5600 cm^{-1} region, three bands due to water dimer were observed.[1] The full width at half-maximum (fwhm) of these stretch−bend dimer transitions was reported to be in the range 36−56 cm^{-1}. A similar experiment in the fundamental OH-stretching region reported two OH-stretching bands with fwhm widths of 50−60 cm^{-1} and a third weaker band to the blue of these.[2]

The third ambient result was the reported first observation of water dimer in the atmosphere.[24] It has been suggested that atmospheric detection of water dimer would be facilitated by probing regions outside of strong monomer absorption. In the third OH-stretching overtone region around 13220−13430 cm^{-1}, the absorption by water monomer is limited and the third OH-stretching overtone of the hydrogen bonded OH-stretching mode in water dimer was predicted by calculations to be in this region.[4] Pfeilsticker et al. reported the observation of a band at 13342 cm^{-1} with a fwhm of 19.4 cm^{-1}. This band showed the expected quadratic dependence on the water monomer partial pressure and had an energy close to that predicted by the previous calculations.[4] The narrow width of the atmospheric observation has been questioned in the literature.[25,26] The widths of OH-stretching transitions at ambient temperatures are typically 25−40 cm^{-1} with hydrogen bonded OH-stretching overtone transitions typically wider.[27–31] In addition, a recent cavity ringdown laboratory experiment in this region[32] measured a number of new water lines not included in the HITRAN version used in ref 24. The new water lines lead to

* To whom correspondence should be addressed. E-mail: henrik@chemistry.otago.ac.nz. Fax: 64-3-479-7906. Phone: 64-3-479-5378.

10.1021/jp802001g CCC: $40.75
Published on Web 07/18/2008

an additional absorbance of similar magnitude to the water dimer absorbance reported in ref 24. Finally, subsequent atmospheric measurements were not able to confirm the first observation, and the result has been revoked.[33]

In previous calculations of OH-stretching overtone transitions in water dimer, coupling to low-frequency modes and the band profiles were ignored.[3,4] The focus in these calculations was the position and overall intensity of the band. However, simulations of the effect of band profiles on absorption of solar radiation have shown that the width and shape of the bands are important.[5] Thus, to shed additional light on the ambient water dimer spectra, we have investigated the band profiles of the OH-stretching transitions in water dimer.

Previously, adiabatic separation of high-frequency XH-stretching vibrations, where X is C, O, or N, from low-frequency internal rotation or torsion have been used to successfully model XH-stretching overtone spectra of a range of molecules such as toluene, peroxynitrous acid, aniline, and methanol.[34–43] In this article we have used a similar approach to calculate the OH-stretching band profiles in water dimer. We use a local mode model that includes an OH-stretching vibration and the low-frequency OO-stretching vibration, which takes place in an effective potential that depends on the OH-stretching state. We simulate band profiles of the OH-stretching transitions by convoluting each of the calculated OO-stretching transitions with an appropriate rotational profile. We have used the coupled cluster with singles, doubles and perturbative triples ab initio method with an augmented triple-ζ correlation consistent basis set to obtain the necessary parameters, potentials, and dipole moment functions.

Theory and Calculations

The dimensionless oscillator strength f of a transition from a ground state g to an excited state e is given by[44]

$$f_{eg} = 4.70165 \times 10^{-7}[\mathrm{cmD}^{-2}]\tilde{\nu}_{eg}|\vec{\mu}_{eg}|^2 \quad (1)$$

where the transition dipole moment ($\vec{\mu}_{eg}$) is expressed in Debye (1 D $\approx 3.33564 \times 10^{-30}$ Cm) and the transition wavenumber ($\tilde{\nu}_{eg}$) in cm^{-1}.

Vibrational Hamiltonian. Our model Hamiltonian includes either the hydrogen bonded (OH_b) or the free (OH_f) OH-stretching vibrational mode of the water dimer proton donor unit and the intermolecular OO-stretching vibrational mode. We have adiabatically separated the high energy OH-stretching mode from the low energy OO-stretching mode. We first determine the OH-stretching vibrational solutions and, for each of these eigenstates, find the OO-stretching solutions. We define the internal displacement coordinates of the OH- and OO-stretching modes as q and s, respectively.

We treat the two OH-stretching local modes in the proton donor unit of water dimer as uncoupled Morse oscillators. This is a reasonable approximation as three-dimensional (3D) calculations on the donor unit including OH_b- and OH_f-stretching and HOH bending modes show the OH_b- and OH_f-stretching eigenstates to be rather pure.[18,45] The Hamiltonian for the OH-stretching mode is diagonal with elements

$$H_{OH}/hc = \left(v + \frac{1}{2}\right)\tilde{\omega} - \left(v + \frac{1}{2}\right)^2 \tilde{\omega}x \quad (2)$$

where v is the vibrational quantum number. The harmonic wavenumber is given by

$$\tilde{\omega} = \frac{\sqrt{g_{ii} f_{ii}}}{2\pi c} \quad (3)$$

where f_{ii} is the second-order force constant and g_{ii} is Wilson's G-matrix element.[46] The anharmonicity parameter is given by[47]

$$\tilde{\omega}x = \frac{\hbar g_{ii}}{2\pi c f_{ii}}\left(\frac{5 f_{iii}^{\ 2}}{48 f_{ii}} - \frac{f_{iv}}{16}\right) \quad (4)$$

where f_{iii} and f_{iv} are the third- and fourth-order force constants, respectively. The force constants are obtained from ab initio calculated potentials. These potentials are calculated by displacing the OH bond from -0.3 to $+0.4$ Å (1 Å $= 10^{-10}$ m) around equilibrium in 0.05 Å steps (15 points). The force contants are found using standard numerical techniques as derivatives of the potential around equilibrium.[48] The grid size used was found to yield converged force constants.

We write the Hamiltonian of the OO-stretching mode for a given OH-stretching vibrational state, v as[37]

$$H_{OO}^{(v)}/hc = T_{OO} + V_{OO}(s) + \left(v + \frac{1}{2}\right)\boldsymbol{\Omega F} - \left(v + \frac{1}{2}\right)^2 \boldsymbol{XF}$$
$$= T_{OO} + V_{OO}^{(v)}(s) \quad (5)$$

where T_{OO} is the kinetic energy operator and $V_{OO}(s)$ is the ab initio calculated OO-stretching potential. The dependence of the OH-stretching harmonic wavenumber and anharmonicity on the OO displacement is approximated by a third-order polynomial in the s coordinate. The coefficients of the polynomial fits are contained in the vectors Ω and $\boldsymbol{X}$ for the harmonic wavenumber and anharmonicity, respectively, and are multiplied by a column vector $\boldsymbol{F} = [1, s, s^2 s^3]^{\mathrm{T}}$. Combining the $V_{OO}(s)$, Ω, and $\boldsymbol{X}$ terms gives the effective OO-stretching potential, $V_{OO}^{(v)}(s)$.

We calculate the OO-stretching potential by displacing s in 0.05 Å steps about equilibrium between -0.4 and $+0.5$ Å (19 points). For each of these OO displacements, the water dimer geometry is partially optimized by allowing the OH bond lengths and HOH angles to optimize, while keeping the coordinates associated with the low-frequency modes fixed. For each of these partially optimized geometries, we calculate OH-stretching grids as described previously to determine the harmonic wavenumber and anharmonicity of the OH-stretching mode.

The effective OO-stretching potentials, $V_{OO}^{(v)}(s)$, deviate significantly from a Morse potential. The eigenfunctions of the effective OO-stretching potentials are obtained from a numerical solution to the one-dimensional Schrödinger equation.[49] We found that the resulting energy levels were converged to within 0.02 cm^{-1} and that the OO-stretching matrix elements $\langle n'|s^j|n\rangle$, $j = 1-5$, where n and n' are the vibrational quantum numbers of the OO-stretching ground and excited states, respectively, were converged to within 1%.

To determine transition intensities, we need to calculate the necessary transition dipole moment (TDM) matrix elements

$$\langle n'\ v|\vec{\mu}(q,s)|n\ 0\rangle \quad (6)$$

where $\vec{\mu}(q,s)$ is the dipole moment function in the OH- and OO-stretching displacement coordinates. The direction of this TDM relative to the rotational axes is necessary for the simulation of rotational structure of each vibrational transition as it provides the A, B, and C rotational band type ratio. In principle an Eckart axis system should be used to minimize vibration−rotation interactions, however it is expected to have only a small effect for water dimer.[45,50]

Dipole Moment Function. We write the dipole moment function (DMF) for the two-coordinate system as

$$\vec{\mu}(q,s) = \sum_{ij} \vec{\mu}_{ij} q^i s^j \quad (7)$$

where the expansion in eq 7 is limited to sixth-order terms diagonal in q ($j = 0$) and off-diagonal terms with $i = 1-4$ and $j = 1$. Terms diagonal in s ($i = 0$) have no contribution to the

intensity of OH-stretching transitions. Terms diagonal in q are determined using a sixth-order polynomial fit to the calculated 15 point OH-stretching grids. This grid size has previously been shown to provide well-converged DMF derivatives and hence intensities.[37] Terms diagonal in q were calculated for each of the OH-stretching grids associated with the different OO displacements. The off-diagonal expansion coefficients are found by standard numerical techniques as the first derivative ($j = 1$) of the diagonal OH-stretching dipole moment expansion coefficients with respect to s.[48] We have inspected the magnitude of the matrix elements, $\langle v'|q^i|0\rangle$ and $\langle n'|s^j|n\rangle$ to select the cutoff value of i and j. These matrix elements and the expansion coefficients of the DMF are given in the Supporting Information.

Spectral Simulation. At ambient temperatures, the population of several of the lowest energy OO-stretching states in the OH-stretching ground-state is significant. We include OO-stretching states up to $n = 3$ and find that including the four lowest states accounts for more than 90% of the population of the OO-stretching states associated with the OH_f- and OH_b-stretching ground states. We allow transitions between all combinations of ground and excited OO-stretching states, resulting in 16 possible OO-stretching transitions for each OH-stretching transition. We scale the calculated intensities of the OO-stretching transitions by the relative Boltzmann population of the OO-stretching states in the OH-stretching ground-state at 298 K.

We have simulated the rotational profile of each of the OO-stretching transitions within a given OH-stretching transition. The TDM does not change significantly between OO-stretching transitions within a given OH-stretching transition and we simulate each OO-stretching transition within a given OH-stretching transition with the rotational band structure of the pure OH-stretching transition. The spectra were simulated using a rigid asymmetric rotor model with a temperature of 298 K. We have used the experimental B and C rotational constants and the calculated A rotational constant for the ground state.[12] For the excited-state we have estimated rotational constants based on previous work.[51] The calculated absorption spectrum was constructed by convoluting each rotational transition with a Lorentzian line shape function with a fwhm of 0.1 cm^{-1}. This line width represents a minimum rotational line width one would expect for water dimer.[12]

Ab Initio Calculations. We have used the coupled cluster including singles, doubles, and perturbative triples [CCSD(T)] method with an augmented triple-ζ correlation consistent basis set (aug-cc-pVTZ) in all ab initio calculations of potential energy and dipole moment functions. All calculations assume a frozen core (O:1s). Calculations were performed using MOLPRO 2002.6.[52] The convergence criteria in the geometry optimization were set to gradient $= 1 \times 10^{-6}$ a.u., step size $= 1 \times 10^{-6}$ a.u., and energy $= 1 \times 10^{-8}$ a.u. In the single point energy calculations for the potential energy and dipole moment functions, the convergence was set to energy $= 1 \times 10^{-10}$ a.u., orbital $= 1 \times 10^{-9}$ a.u., and coeff $= 1 \times 10^{-8}$ a.u. The dipole moments were calculated as first derivatives with respect to an applied finite field. The field strength used was 0.00015 a.u.

Results and Discussion

The CCSD(T)/aug-cc-pVTZ equilibrium geometry of $H_2O \cdot H_2O$ is shown in Figure 1. The geometry agrees with previous calculations and the experimentally determined geometry.[3,4,53,54] The partially optimized geometries at each fixed OO distance are given in the Supporting Information.

Local Mode Parameters. The variation of the harmonic wavenumber and anharmonicity parameter of the OH_b- and OH_f-stretching modes with s are shown in Figure 2. The third order polynomial fits to these points are also shown and the coefficients of these polynomial fits are given in Table 1. The OH_b-stretching potential is strongly affected by the change in s with $\tilde{\omega}_b$ changing by around 50 cm^{-1} and $\tilde{\omega}x_b$ by around 25 cm^{-1} whereas the local mode parameters for the OH_f-stretching mode show significantly less variation with s. Both OH-stretching potentials become more anharmonic as the OO separation is reduced.

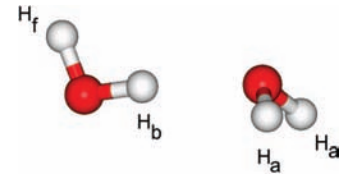

Figure 1. CCSD(T)/aug-cc-pVTZ optimized structure of water dimer.

OO-Stretching Transitions. The effective OO-stretching potentials associated with the OH_b-stretching states $v_b = 0-5$ are shown in Figure 3. These potentials change significantly with v_b. The minimum of each effective potential is displaced from that of the ab initio calculated OO-stretching potential and occurs at more compressed OO distances as v_b increases. This will significantly affect the positions and intensities of the OO-stretching transitions. The OO-stretching potentials associated with the different v_f states are almost identical and are given in the Supporting Information. The displacement of the minimum for each of the effective OO-stretching potentials are given in the Supporting Information.

We have calculated the transition wavenumbers and intensities of the OO-stretching transitions within each OH-stretching transition according to eq 1. These are given in the Supporting Information and are shown as vertical lines in Figures 4–8. For comparison, the wavenumber of the pure OH-stretching transition obtained from a one-dimensional (1D) calculation is shown as a dashed line. All figures are shown with the same range of the wavenumber axis. As a result of the very small change in the effective OO-stretching potentials associated with the ground and excited OH_f-stretching states, only OO-stretching transitions $n' \leftarrow n$ where $n = n'$ have significant intensity. For each OH_f-stretching transition $\Delta v_f = 1-5$ the $n' = 0 \leftarrow n = 0$, OO-stretching transition is the most intense, followed by the hot bands from $n = 1$, 2, and 3 with $\Delta n = n' - n = 0$.

For the OH_b-stretching states a very different picture emerges due to the relative displacement of the effective potentials. In this case, many transitions $n' \leftarrow n$ where $\Delta n \neq 0$ also have appreciable intensity. The general result of this is that the intensity of the OH_b-stretching transition is distributed over a larger number of OO-stretching transitions and hence a larger wavenumber range. Interestingly, the $n' = 0 \leftarrow n = 0$ transition does not have the same energy as the pure OH-stretching transition because of the relative energy displacement of the effective OO-stretching potential minima.

For the fundamental OH_b-stretching state (Figure 4), the four most intense OO-stretching transitions are those where $\Delta n = 0$, as expected from the relatively small change in the effective OO-stretching potential. As such, the distribution of intensity of the fundamental OH_b- and OH_f-stretching transitions is similar. In agreement with previous studies, for the first OH_b-stretching overtone transition ($\Delta v_b = 2$), there is a near-cancelation of terms within the TDM matrix element in the q coordinate.[55] Consequently, more terms in the TDM matrix element contribute significantly to the intensity and the intensi-

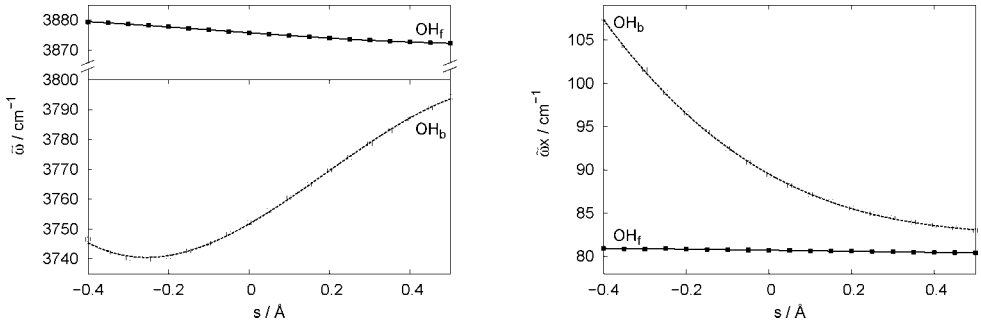

Figure 2. Variation of $\tilde{\omega}$ (left) and $\tilde{\omega}x$ (right) with O−O displacement. The local mode parameters associated with the OH_b -stretching mode are shown with open squares and dashed lines. The local mode parameters associated with the OH_f-stretching mode are shown with filled squares and solid lines.

TABLE 1: Coefficients of the Polynomial Expansion of the OH-Stretching Harmonic Wavenumber (Ω) and Anharmonicity (X)[a]

	OH_b		OH_f	
	Ω	X	Ω	X
$1/cm^{-1}$	3751.69	89.52	3875.80	80.74
s/cm^{-1} Å^{-1}	77.53	− 26.66	− 9.62	− 0.54
s^2/cm^{-1} Å^{-2}	91.59	37.07	1.98	0.37
s^3/cm^{-1} Å^{-3}	− 157.91	− 19.13	6.47	− 0.04

[a] From a third-order linear least-squares polynomial fit to the calculated local mode parameters.

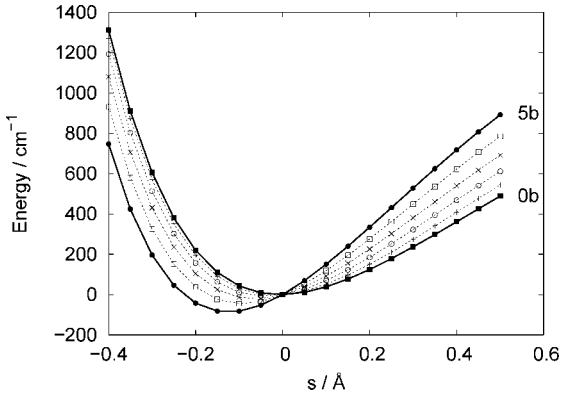

Figure 3. Effective OO-stretching potentials associated with OH_b-stretching states. ■, $V_{OO}^{(0b)}$; +, $V_{OO}^{(1b)}$; ⊙, $V_{OO}^{(2b)}$; ×, $V_{OO}^{(3b)}$; ⊡, $V_{OO}^{(4b)}$; ●, $V_{OO}^{(5b)}$. The superscripts refer to the number of quanta in the OH_b-stretching mode.

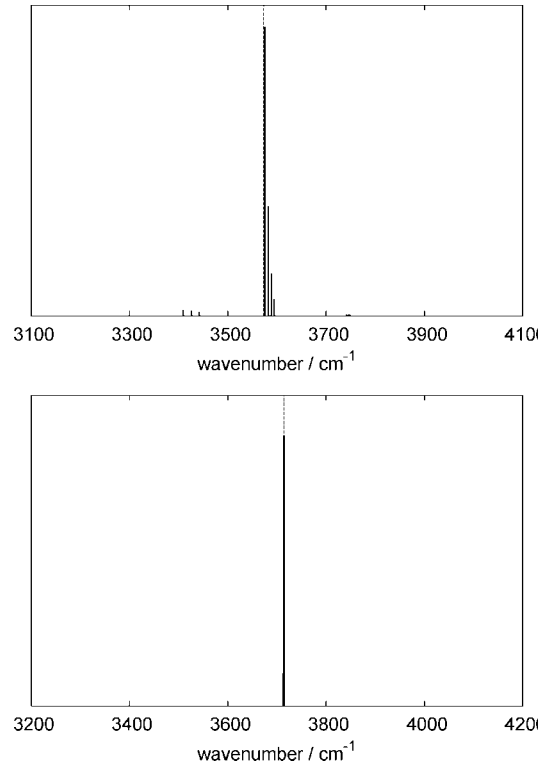

Figure 4. Calculated OO-stretching transitions within the $\Delta v_b = 1$ (top) and $\Delta v_f = 1$ (bottom) transitions in water dimer ($T = 298$ K). The dashed line indicates the position of the OH-stretching transition from a 1D calculation.

ties of most of the 16 OO-stretching transitions considered are of similar order. As shown in Figure 5, the intensity of the $\Delta v_b = 2$ band is distributed over several OO-stretching transitions, however due to the cancelation of terms all transitions are relatively weak. The band is dominated by the $\Delta n = +1$ transitions which have similar energies and appear as a group of bands at ∼7150 cm^{-1}. It is worth noting that these bands are shifted ∼150 cm^{-1} to the blue of the pure OH_b-stretching transition. There is a similar group of bands at ∼7000 cm^{-1} corresponding to transitions where $\Delta n = 0$ and at ∼6800 cm^{-1} arising from transitions where $\Delta n = -1$. A similar grouping of transitions is seen for the $\Delta v_b = 3$ band (Figure 6), with transitions spread slightly wider. For the $\Delta v_b = 4$ and 5 bands (Figures 7 and 8), we find that the $n' = 0 \leftarrow n = 0$ transition is the most intense, with the $\Delta n = +1$ transitions also making significant contributions to the intensity. The intensity is distributed over a large wavenumber range for both of these OH_b-stretching overtone transitions.

We have compared the sum of the intensities of each OO-stretching transition within a given OH-stretching transition with that obtained from a 1D OH-stretching calculation in Table 2. We find that the total intensity calculated with the 1D and 2D models are similar for the OH_f-stretching transitions. For the OH_b -stretching transitions the variation is larger but still within 30% of each other for the $\Delta v_b = 1$, 4, and 5 transitions. For the $\Delta v_b = 2$ and 3 transitions the cancelation of terms and the weaker intensity makes them more sensitive to perturbation. The minimal change in intensity upon inclusion of the OO-stretching mode indicates that the total intensity is reasonably well described by a purely OH-stretching model and that, as expected, the OH-stretching bright state carries most of the intensity. The effect of including the OO-stretching mode is to distribute the intensity of the OH-stretching transition over a substantial wavenumber range, rather than to change the total band intensity. Coupling between the OH_b- and OH_f-stretching modes would change the intensity of the bands. The effect of this is largest for the fundamental region and decreases with overtone, as can be seen from comparison with recent calculations that include coupling between the OH-stretching modes.[45]

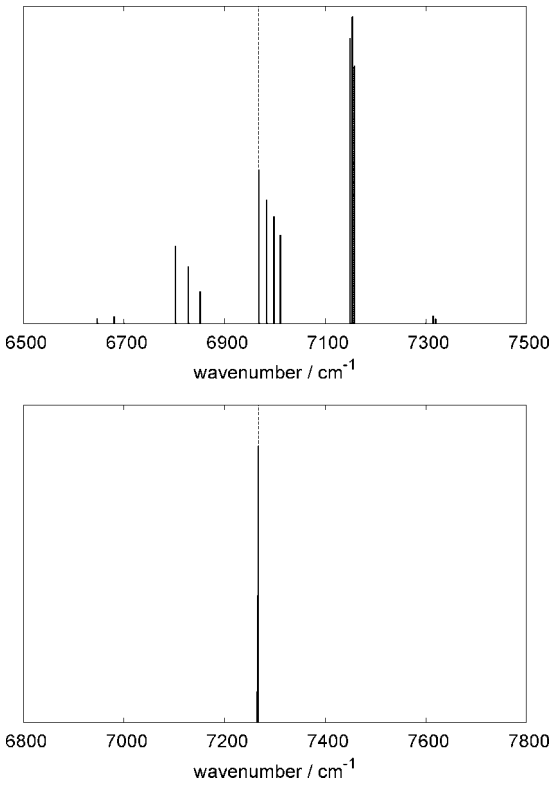

Figure 5. Calculated OO-stretching transitions within the $\Delta v_b = 2$ (top) and $\Delta v_f = 2$ (bottom) transitions in water dimer ($T = 298$ K). The dashed line indicates the position of the OH-stretching transition from a 1D calculation.

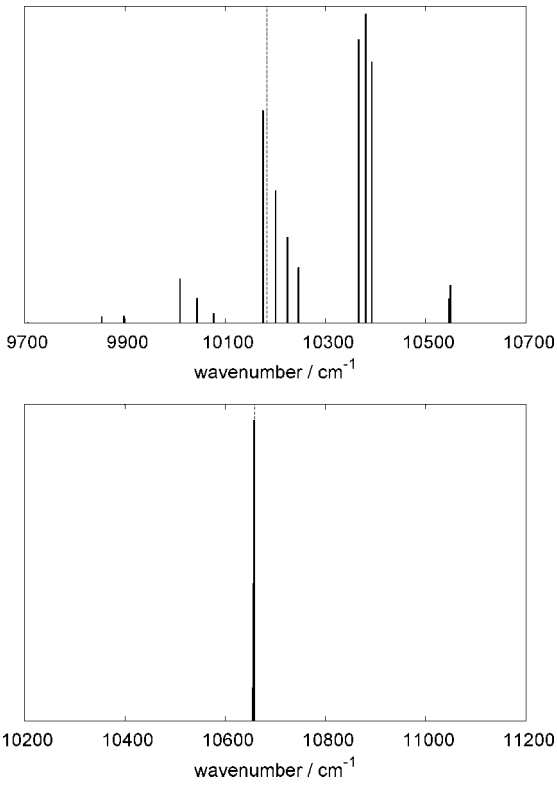

Figure 6. Calculated OO-stretching transitions within the $\Delta v_b = 3$ (top) and $\Delta v_f = 3$ (bottom) transitions in water dimer ($T = 298$ K). The dashed line indicates the position of the OH-stretching transition from a 1D calculation.

Simulated Spectra. We have used the TDMs and the rotational constants to simulate the rotational transitions associated with each of the OO-stretching transitions within the given OH-stretching transition. The direction of the TDM with respect to the rotational axes determines the mix of the rotational band type. For water dimer we find that all transitions are $A-B$ hybrids with the mix dependent on the vibrational state. A and B type transitions have different band shapes, which leads to the various vibrational transitions having different rotational profiles. A previous microwave study of water dimer found the B rotational axis to lie perpendicular to the symmetry axis of the molecule and the C axis to lie in this plane,[56] contrary to what is calculated in this work. However, the B and C rotational constants are almost identical, and a small change in structure can interchange the axes. Indeed, when the geometry of water dimer is optimized using a smaller double-ζ basis set, we observe such an effect. If the axes are interchanged the individual bands will be $A-C$ hybrids rather than the $A-B$ hybrids found in this work. We have also simulated the bands with an $A-C$ type structure and find there is no visible difference in the resulting spectra. We find that if we use the TDM calculated for each individual OO-stretching transition rather than the pure OH-stretching TDM there is little difference in the resulting spectrum. The directions of the strongest OO-stretching TDMs are similar to the direction of the pure OH-stretching TDM. The TDMs of the weak OO-stretching transitions differ more from the pure OH-stretching TDM. The TDMs for each OO-stretching transition are given in the Supporting Information.

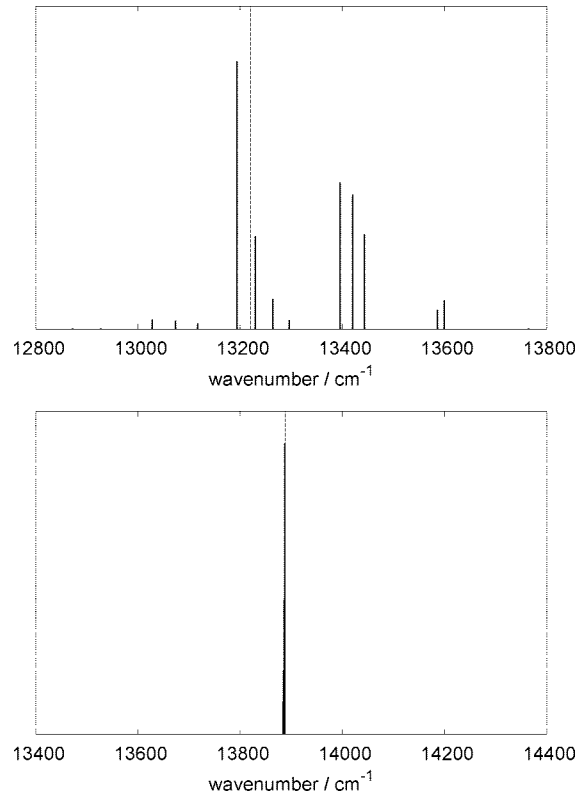

Figure 7. Calculated OO-stretching transitions within the $\Delta v_b = 4$ (top) and $\Delta v_f = 4$ (bottom) transitions in water dimer ($T = 298$ K). The dashed line indicates the position of the OH-stretching transition from a 1D calculation.

We present the simulated spectra of the fundamental OH_b- and OH_f-stretching transitions in Figure 9. We have simulated these spectra with a value of the equilibrium constant of dimerization (K_{eq}) of 0.04 atm^{-1}, $T = 298$ K and a water vapor pressure $p_{H_2O} = 14.4$ mbar. The temperature and pressure are similar to the parameters of the recent ambient experiments.[1,2,24,32]

TABLE 2: Energies (in cm^{-1}) and Oscillator Strengths of the OH-Stretching Transitions

	OH_b			OH_f		
v	E^a	$f_{1D}{}^a$	$f_{2D}{}^b$	E^a	$f_{1D}{}^a$	$f_{2D}{}^b$
1	3573.28	6.86×10^{-5}	6.15×10^{-5}	3714.25	2.95×10^{-6}	3.10×10^{-6}
2	6967.76	6.60×10^{-9}	3.66×10^{-8}	7267.01	2.96×10^{-7}	2.98×10^{-7}
3	10183.44	1.01×10^{-9}	3.22×10^{-9}	10658.30	9.30×10^{-9}	9.33×10^{-9}
4	13220.30	2.96×10^{-10}	3.84×10^{-10}	13888.10	4.05×10^{-10}	4.09×10^{-10}
5	16078.37	4.65×10^{-11}	4.48×10^{-11}	16956.42	3.32×10^{-11}	3.37×10^{-11}

[a] From a 1D calculation. [b] Sum of the OO-stretching transitions within a given band.

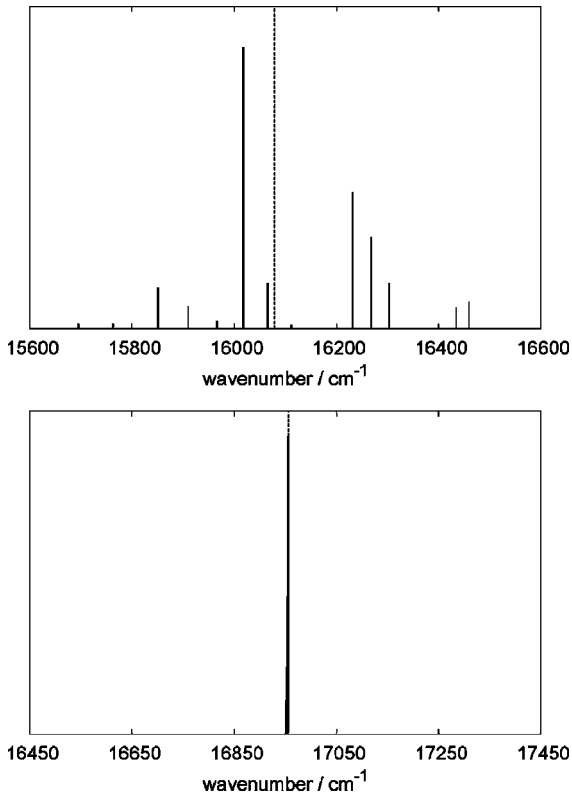

Figure 8. Calculated OO-stretching transitions within the $\Delta v_b = 5$ (top) and $\Delta v_f = 5$ (bottom) transitions in water dimer ($T = 298$ K). The dashed line indicates the position of the OH-stretching transition from a 1D calculation.

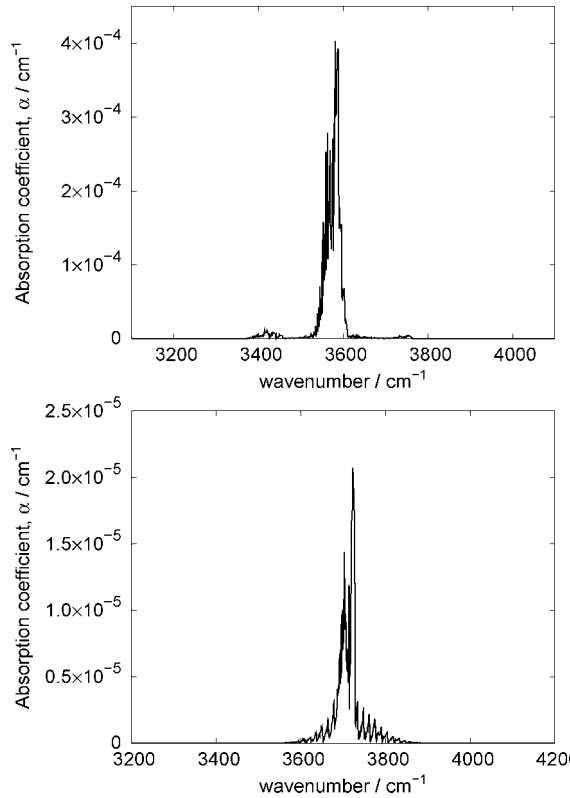

Figure 9. Simulated spectra of $\Delta v_b = 1$ (top) and $\Delta v_f = 1$ (bottom) transitions in water dimer. Simulated for $T = 298$ K, $p_{H_2O} = 14.4$ mbar and $K_{eq} = 0.04$ atm^{-1}. Each rotational line is convoluted with a Lorentzian function with a fwhm of 0.1 cm^{-1}.

The equilibrium constant is not known accurately, but the range of results in the literature is 0.01−0.1 atm^{-1}, from both experiment and a range of theoretical predictions.[1,2,57–60] As mentioned in the Theory section, we have used a Lorentzian line shape with a fwhm of 0.1 cm^{-1}.[12,61] In a recent jet-cooled experiment of the first OH-stretching overtone region rotational linewidths of ∼0.25 cm^{-1} were observed.[14] Very recently jet-cooled high OH-stretching overtone spectra of methanol showed minimum linewidths of 0.5 cm^{-1}.[42] This wider line width arises from intramolecular vibrational redistribution (IVR). In addition to our 0.1 cm^{-1} line width, we have simulated spectra using 0.5 and 1.0 cm^{-1} Lorentzian lineshapes. We present these spectra in the Supporting Information. The increased line width has little effect on the overall bandwidth, but decreases the absorptivity as expected. Even wider linewidths are conceivable in water dimer which is likely to have faster IVR than, for example, methanol.[42]

The direction of the TDM of the fundamental OH-stretching transitions and the rotational axes are shown in Figure 10. As seen in Figure 4, there is limited OO-stretching vibrational structure in the fundamental OH-stretching spectra and the band profiles will be dominated by rotational structure. The TDM of the fundamental OH_b-stretching transition lies predominantly along the A rotational axis and as such, the resulting OH_b-stretching spectrum shows mostly A-type structure. The OO-stretching transitions with $\Delta n = -1$, give rise to a weak band around 3425 cm^{-1}. The TDM of the fundamental OH_f-stretching transition has comparable A and B components and the resulting spectrum shows both A- and B-type rotational structure. Thus the two fundamental OH-stretching bands have somewhat different band profiles. However, the overall width of the OH-stretching band is around 35 cm^{-1} for both fundamental transitions.

The fundamental region of the water dimer spectrum has recently been recorded in the gas phase at atmospherically relevant conditions.[2] Two main peaks due to water dimer were observed, with the lower energy band assigned to the fundamental OH_b-stretching transition, and the higher energy transition assigned to the OH_f-stretching and asymmetric acceptor stretching modes.[2,3] At slightly higher energy, weaker combination peaks are observed.[2,45] Both of the observed main peaks were found to have fwhm band widths of ∼50−60 cm^{-1}. An analogous experiment in the 5000−5600 cm^{-1} region found peaks with fwhm band widths of ∼30−50 cm^{-1} and assigned

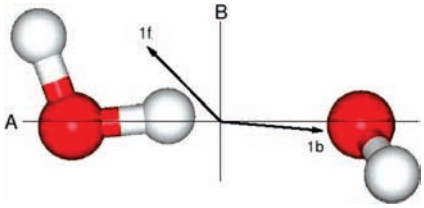

Figure 10. Calculated TDM of the fundamental OH_b- and OH_f-stretching trantions in water dimer. The *A* and *B* rotational axes are shown.

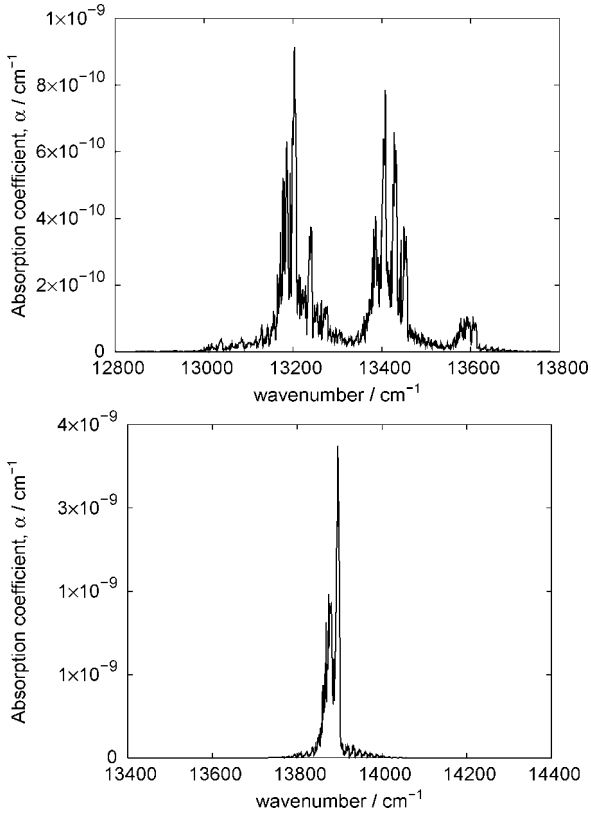

Figure 11. Simulated spectra of $\Delta v_b = 4$ (top) and $\Delta v_f = 4$ (bottom) transitions in water dimer. Simulated for $T = 298$ K, $p_{H_2O} = 14.4$ mbar and $K_{eq} = 0.04$ atm^{-1}. Each rotational line is convoluted with a Lorentzian function with a fwhm of 0.1 cm^{-1}.

them to stretch−bend water dimer transitions.[1] The observed band widths are in good agreement with our calculated widths. We find that our calculated peak heights differ somewhat from those observed.[2] The simulation in Figure 9 is also shown in the Supporting Information with the cm^2 molecule^{-1} atm^{-1} units, which were used in the experiment.[2] Compared with experiment, the calculated OH_b-stretching transition is around five times more intense, and the OH_f-stretching transition half as intense. However, in our model the two OH-stretching modes are treated as uncoupled Morse oscillators. In the fundamental region, coupling between the two OH-stretching modes will lower the intensity of the OH_b-stretching transition and increase the intensity of the OH_f -stretching transition via mixing.[18,45] This is less important for the higher energy transitions as local modes have been shown to become more localized as the energy increases.[62]

The simulated spectra of the third overtone OH-stretching transitions are shown in Figure 11 and the TDM of each of the OH-stretching transitions shown in Figure 12. We have simulated these transitions with the same parameters used in the fundamental spectra. Rotation of the TDM with vibrational

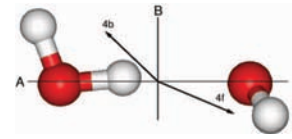

Figure 12. Calculated TDM of the third overtone OH_b- and OH_f-stretching trantions in water dimer. The *A* and *B* rotational axes are shown.

transition has been observed previously and also occurs for water dimer.[29,63–66] In the third overtone transition, the OH_f-stretching mode has the TDM predominantly along the *A* axis and thus exhibits mostly *A*-type structure. The only OO-stretching transitions within the third overtone OH_f-stretching transitions with appreciable intensity are those with $\Delta n = 0$, and as seen in Figure 7 these all have similar energies (within 4 cm^{-1}). The structure of this band arises mainly from rotational transitions and the width is similar to that of the fundamental transition with a fwhm of ~40 cm^{-1}.

In contrast, the OH_b-stretching transition is an *A*−*B* hybrid, with the direction of its TDM similar to that of the OH_f-fundamental. Many of the OO-stretching transitions within the third OH_b-stretching overtone transition have significant intensity, as seen in Figure 7. As a result the OH_b-stretching band appears as several peaks spread over a substantial wavenumber range, and the overall profile is significantly widened compared to the third overtone OH_f-stretching transition. The intensity of the third overtone OH_f- and OH_b-stretching transition are similar and thus, as the width of the band increases the maximum absorbance decreases, as seen clearly in Figure 11. This is one of the reasons why detection of OH_b-stretching overtone transitions in water dimer has been elusive.

Water vapor was measured in the atmosphere in the 13220−13430 cm^{-1} region and a peak observed at 13342 cm^{-1} with a fwhm of 19.4 cm^{-1} was assigned to the third overtone OH_b-stretching transition in water dimer.[24] The atmospheric experiment has since been revisited and additional measurements were taken under conditions more favorable to dimer formation.[33] No spectral features near 13342 cm^{-1} that could be assigned to water dimer were observed and the authors conclude their previous observation was probably not due to water dimer.[33] Our simulated OH-stretching band profiles show that absorption due to water dimer in this region is likely very broad, spanning several hundreds of cm^{-1} with a low maximum absorbance.

The absorption spectrum of water vapor in the region 13312.4−13377.7 cm^{-1} has been measured using cavity ring down spectroscopy (CRDS) in the laboratory under ambient conditions.[32] The typical sensitivity in the CRDS experiment was 3×10^{-10} cm^{-1}, which allowed detection of hundreds of additional weak water lines. The CRDS measurements were taken over a series of around eighty 1 cm^{-1} intervals making detection of a broad band difficult.

Our model only includes one OH-stretching mode and the OO-stretching mode, instead of all twelve vibrational modes. A harmonic frequency calculation on water dimer indicates that two of the intermolecular normal modes involve OO-stretching motion mixed with the acceptor unit wag and, to a lesser extent, the donor unit rock. We suspect that these intermolecular vibrations will also contribute to the OH-stretching band profile. The inclusion of other intermolecular modes would result in additional transitions likely located in a similar wavenumber range to those we have calculated and would add complexity to our simulated spectra and further distribute the intensity of

the OH-stretching bright states. This would lead to a water dimer OH_b-stretching third overtone profile that is a broad band spanning several hundreds of wavenumbers and with a low maximum absorption. This is a likely reason for the difficulties associated with observing the OH_b-stretching overtone transitions in water dimer and other complexes.[27,67]

Conclusions

We have calculated band profiles of the OH-stretching transitions in the proton donor unit of water dimer. We have used a local mode Hamiltonian which includes the low energy OO-stretching mode and the high energy OH-stretching modes, but separates these adiabatically. We have included the variation of OH-stretching harmonic wavenumber and anharmonicity with OO displacement to construct effective OO-stretching potentials associated with each of the OH-stretching states. Transitions between the resulting OO-stretching energy levels in the ground and excited OH-stretching states were used to calculate the band profile for each of the OH-stretching transitions. The individual OO-stretching transitions were convoluted with the calculated rotational profile of the OH-stretching transition.

In the fundamental region, we find that the free OH-stretching (OH_f) and hydrogen bonded OH-stretching (OH_b) transitions are dominated by only a few OO-stretching transitions. The calculated widths of the associated band profiles are $\sim$35 cm^{-1}, in agreement with the available gas phase data. The OH_f- and OH_b-stretching band profiles become more and more different as the vibrational excitation increases. For the OH_b-stretching mode an increasing number of OO-stretching transitions have appreciable intensity as the vibrational energy increases. As a consequence, the intensity of a given OH_b-stretching overtone transition is distributed over many OO-stretching transitions. These transitions are spread over a wide energy range, which results in a broad OH_b-stretching band profile with an overall width of around 300 cm^{-1} for the third overtone. The vibrational profiles of the OH_f-stretching transitions do not broaden markedly with increasing overtone and the third overtone OH_f-stretching transition has a width of around 40 cm^{-1}.

As a result of the very broadband profile of the third OH_b-stretching overtone transition its maximum absorbance is low. This is likely one of the reasons why higher overtone OH_b-stretching transitions in water dimer have been elusive.

Acknowledgment. We are grateful to Jeppe Olsen for use of his ONEDIM program. We would like to thank Alain Campargue, Poul Jørgensen, Klaus Pfeilsticker, and Igor Ptashnik for helpful discussions. H.G.K. is grateful to Aarhus University Research Foundation for a visiting professorship. We acknowledge the Marsden Fund administered by the Royal Society of New Zealand, the Lundbeck Foundation, the Academy of Finland, and the Universities of Helsinki and Otago for financial support.

Supporting Information Available: The partially optimized geometries of $H_2O \cdot H_2O$ in Z-matrix format. The energy and coordinate displacements of each OO-stretching effective potential relative to the ab initio OO-stretching potential. Effective OO-stretching potentials associated with OH_f-stretching states. Transition dipole moments of OO-stretching transitions within the $v = 1$ and $v = 4$ OH-stretching transitions. The OH- and OO-stretching matrix elements, $\langle v'|q^i|0\rangle$ and $\langle n'|s^j|n\rangle$. The expansion coefficients of the dipole moment function. The energies and intensities of OO-stretching transitions. The simulated spectra of the fundamental OH_b- and OH_f-stretching transitions, simulated using the units of ref 2. The simulated spectra of the fundamental OH_b- and OH_f-stretching transitions, simulated using 0.5 and 1.0 cm^{-1} (fwhm) lineshapes. This material is available free of charge via the Internet at http://pubs.acs.org.

References and Notes

(1) Ptashnik, I. V.; Smith, K. M.; Shine, K. P.; Newnham, D. A. *Q. J. R. Meteorol. Soc.* **2004**, *130*, 2391–2408.
(2) Paynter, D. J.; Ptashnik, I. V.; Shine, K. P.; Smith, K. M. *Geophys. Res. Lett.* **2007**, *34*, LI2808.
(3) Schofield, D. P.; Kjaergaard, H. G. *Phys. Chem. Chem. Phys.* **2003**, *5*, 3100–3105.
(4) Low, G. R.; Kjaergaard, H. G. *J. Chem. Phys.* **1999**, *110*, 9104–9115.
(5) Vaida, V.; Daniel, J. S.; Kjaergaard, H. G.; Goss, L. M.; Tuck, A. F. *Q. J. R. Meteorol. Soc.* **2001**, *127*, 1627–1643.
(6) Perchard, J. P. *Chem. Phys.* **2001**, *273*, 217–233.
(7) Perchard, J. P. *Chem. Phys.* **2001**, *266*, 109–124.
(8) Bouteiller, Y.; Perchard, J. P. *Chem. Phys.* **2004**, *305*, 1–12.
(9) Hirabayashi, S.; Yamada, K. M. T. *J. Chem. Phys.* **2005**, *122*, 244501.
(10) Burnham, C. J.; Xantheas, S. S.; Miller, M. A.; Applegate, B. E.; Miller, R. E. *J. Chem. Phys.* **2002**, *117*, 1109–1122.
(11) Fröchtenicht, R.; Kaloudis, M.; Koch, M.; Huisken, F. *J. Chem. Phys.* **1996**, *105*, 6128–6140.
(12) Huang, Z. S.; Miller, R. E. *J. Chem. Phys.* **1989**, *91*, 6613–6631.
(13) Huisken, F.; Kaloudis, M.; Kulcke, A. *J. Chem. Phys.* **1996**, *104*, 17–25.
(14) Nizkorodov, S. A.; Ziemkiewicz, M.; Nesbitt, D. J.; Knight, A. E. W. *J. Chem. Phys.* **2005**, *122*, 194316.
(15) Paul, J. B.; Provencal, R. A.; Chapo, C.; Roth, K.; Casaes, R.; Saykally, R. J. *J. Phys. Chem. A* **1999**, *103*, 2972–2974.
(16) Slipchenko, M. N.; Kuyanov, K. E.; Sartakov, B. G.; Vilesov, A. F. *J. Chem. Phys.* **2006**, *124*, 241101.
(17) Chaban, G. M.; Jung, J.-O.; Gerber, R. B. *J. Chem. Phys.* **1999**, *111*, 1823–1829.
(18) Schofield, D. P.; Lane, J. R.; Kjaergaard, H. G. *J. Phys. Chem. A* **2007**, *111*, 567–572.
(19) Keutsch, F. N.; Braly, L. B.; Brown, M. G.; Harker, H. A.; Petersen, P. B.; Leforestier, C.; Saykally, R. J. *J. Chem. Phys.* **2003**, *119*, 8927–2937.
(20) Leforestier, C.; Gatti, F.; Fellers, R. S.; Saykally, R. J. *J. Chem. Phys.* **2002**, *117*, 8710–8722.
(21) Goldman, N.; Fellers, R. S.; Brown, M. G.; Braly, L. B.; Keoshian, C. J.; Leforestier, C.; Saykally, R. J. *J. Chem. Phys.* **2002**, *116*, 10148–10163.
(22) Smit, M. J.; Groenenboom, G. C.; Wormer, P. E. S.; van der Avoird, A.; Bukowski, R.; Szalewicz, K. *J. Phys. Chem. A* **2001**, *105*, 6212–6225.
(23) Bukowski, R.; Szalewicz, K.; Groenenboom, G. C.; van der Avoird, A. *Science* **2007**, *315*, 1249–1252.
(24) Pfeilsticker, K.; Lotter, A.; Peters, C.; Bösch, H. *Science* **2003**, *300*, 2078–2080.
(25) Suhm, M. A. *Science (Letters)* **2004**, *304*, 823.
(26) Pfeilsticker, K. A. *Science (Letters)* **2004**, *304*, 823–824.
(27) Howard, D. L.; Kjaergaard, H. G. *J. Phys. Chem. A* **2006**, *110*, 9597–9601.
(28) Howard, D. L.; Kjaergaard, H. G. *J. Phys. Chem. A* **2006**, *110*, 10245–10250.
(29) Ishiuchi, S.; Fujii, M.; Robinson, T. W.; Miller, B. J.; Kjaergaard, H. G. *J. Phys. Chem. A* **2006**, *110*, 7345–7354.
(30) Howard, D. L.; Kjaergaard, H. G. *J. Chem. Phys.* **2004**, *121*, 136–140.
(31) Häber, T.; Schmitt, U.; Suhm, M. A. *Phys. Chem. Chem. Phys.* **1999**, *1*, 5573–5582.
(32) Kassi, S.; Macko, P.; Naumenko, O.; Campargue, A. *Phys. Chem. Chem. Phys.* **2005**, *7*, 2460–2467, and private communication with A. Campargue.
(33) Lotter, A. Field Measurements of Water Continuum and Water Dimer Absorption by Active Long Path Differential Optical Absorption Spectroscopy (DOAS). PhD thesis, University of Heidelberg: Heidelberg, Germany, 2006, and private communication with K. Pfeilsticker.
(34) Cavagnat, D.; Lespade, L.; Lapouge, C. *J. Chem. Phys.* **1995**, *103*, 10502–10512.
(35) Zhu, C.; Kjaergaard, H. G.; Henry, B. R. *J. Chem. Phys.* **1997**, *107*, 691–701.
(36) Hänninen, V.; Horn, M.; Halonen, L. *J. Chem. Phys.* **1999**, *111*, 3018–3026.
(37) Rong, Z.; Kjaergaard, H. G. *J. Phys. Chem. A* **2002**, *106*, 6242–6253.

(38) Haynes, L. M.; Vogelhuber, K. M.; Pippen, J. L.; Hsieh, S. *J. Chem. Phys.* **2005**, *123*, 234306.
(39) McCoy, A. B.; Fry, J. L.; Francisco, J. S.; Mollner, A. K.; Okumura, M. *J. Chem. Phys.* **2005**, *122*, 104311.
(40) Schofield, D. P.; Kjaergaard, H. G.; Matthews, J.; Sinha, A. *J. Chem. Phys.* **2005**, *123*, 134318.
(41) Hänninen, V.; Halonen, L. J. *Chem. Phys.* **2007**, *126*, 064309.
(42) Maksyutenko, P.; Boyarkin, O. V.; Rizzo, T. R.; Perry, D. S. *J. Chem. Phys.* **2007**, *126*, 044311.
(43) Dübal, H.-R.; Crim, F. F. J. *Chem. Phys.* **1985**, *83*, 3863–3872.
(44) Atkins, P. W. *Molecular Quantum Mechanics*, 2nd ed.; Oxford University Press: Oxford, U.K., 1983.
(45) Kjaergaard, H. G.; Garden, A. L.; Chaban, G. M.; Gerber, R. B.; Matthews, D. A.; Stanton, J. F. *J. Phys. Chem. A* **2008**, *112*, 4324–4335.
(46) Wilson Jr., E. B. ; Decius, J. C. ; Cross, P. C. *Molecular Vibrations*; Dover Publications, Inc.: New York, 1980.
(47) Howard, D. L.; Jørgensen, P.; Kjaergaard, H. G. *J. Am. Chem. Soc.* **2005**, *127*, 17096–17103.
(48) Press, W. H.; Flannery, B. F.; Teukolsky, S. A.; Vetterling, W. T. *Numerical Recipes in C*; Cambridge University: Cambridge, 1988.
(49) ONEDIM program. Olsen, J. Private communication.
(50) Salmi, T.; Hänninen, V.; Garden, A. L.; Kjaergaard, H. G.; Tennyson, J.; Halonen, L. *J. Phys. Chem. A* **2008**, . *in press*.
(51) Halonen, L.; Duxbury, G. *Chem. Phys. Lett.* **1985**, *118*, 246–251.
(52) MOLPRO, version 2002.6, a package of ab initio programs. Werner, H.-J.; Knowles, P. J.; Lindh, R.; Schütz, M.; Celani, P.; Korona, T.; Manby, F. R.; Rauhut, G.; Amos, R. D.; Bernhardsson, A.; Berning, A.; Cooper, D. L.; Deegan, M. J. O.; Dobbyn, A. J.; Eckert, F.; Hampel, C.; Hetzer, G.; Lloyd, A. W.; McNicholas, S. J.; Meyer, W.; Mura, M. E.; Nicklass, A.; Palmieri, P.; Pitzer, R.; Schumann, U.; Stoll, H.; Stone, A. J.; Tarroni, R.; Thorsteinsson, T. 2003.
(53) Dyke, T. R.; Mack, K. M.; Muenter, J. S. *J. Chem. Phys.* **1977**, *66*, 498–510.
(54) Xantheas, S. S.; Dunning, T. H., Jr. *J. Chem. Phys.* **1993**, *99*, 8774–8792.
(55) Kjaergaard, H. G.; Low, G. R.; Robinson, T. W.; Howard, D. L. *J. Phys. Chem. A.* **2002**, *106*, 8955–8962.
(56) Fraser, G. T.; Suenram, R. D.; Coudert, L. H. *J. Chem. Phys.* **1989**, *90*, 6077–6085.
(57) Scribano, Y.; Goldman, N.; Saykally, R. J.; Leforestier, C. *J. Phys. Chem. A* **2006**, *110*, 5411–5419.
(58) Goldman, N.; Fellers, R. S.; Leforestier, C.; Saykally, R. J. *J. Phys. Chem. A* **2001**, *105*, 515–519.
(59) Goldman, N.; Leforestier, C.; Saykally, R. J. *J. Phys. Chem. A* **2004**, *108*, 787–794.
(60) Curtiss, L. A.; Frurip, D. J.; Blander, M. *J. Chem. Phys.* **1979**, *71*, 2703–2711.
(61) Nesbitt, D. J.; Field, R. W. *J. Phys. Chem.* **1996**, *100*, 12735–12756.
(62) Mortensen, O. S.; Henry, B. R.; Mohammadi, M. A. *J. Chem. Phys.* **1981**, *75*, 4800–4808.
(63) Fair, J. R.; Votava, O.; Nesbitt, D. J. *J. Chem. Phys.* **1998**, *108*, 72–80.
(64) Hurtmans, D.; Herregodts, F.; Herman, M.; Lievin, J.; Campargue, A.; Garnache, A.; Kachanov, A. A. *J. Chem. Phys.* **2000**, *113*, 1535–1545.
(65) Takahashi, K.; Sugawara, M.; Yabushita, S. *J. Phys. Chem. A* **2005**, *109*, 4242–4251.
(66) Konen, I. M.; Li, E. X. J.; Stephenson, T. A.; Lester, M. I. *J. Chem. Phys.* **2005**, *123*, 204318.
(67) Howard, D. L.; Kjaergaard, H. G. *J. Phys. Chem. A* **2006**, *110*, 10245–10250.

JP802001G